Systematic study of $Ga_{1-x}In_xAs$ self-assembled quantum wires with different interfacial strain relaxation

Liang-Xin Li, Sophia Sun and Yia-Chung Chang

Department of Physics and Materials Research Laboratory

University of Illinois at Urbana-Champaign, Urbana, Illinois 61801

(February 1, 2008)

Abstract

A systematic theoretical study of the electronic and optical properties of $Ga_{1-x}In_xAs$ self-assembled quantum-wires (QWR's) made of short-period superlattices (SPS) with strain-induced lateral ordering is presented. The theory is based on the effective bond-orbital model (EBOM) combined with a valence-force field (VFF) model. Valence-band anisotropy, band mixing, and effects due to local strain distribution at the atomistic level are all taken into account. Several structure models with varying degrees of alloy mixing for lateral modulation are considered. A valence force field model is used to find the equilibrium atomic positions in the QWR structure by minimizing the lattice energy. The strain tensor at each atomic (In or Ga) site is then obtained and included in the calculation of electronic states and optical properties. It is found that different local arrangement of atoms leads to very different strain distribution, which in turn alters the optical properties. In particular, we found that in model structures with thick capping layer the electron and hole are confined in the Ga-rich region and the optical anisotropy can be reversed due to the variation of lateral alloying mixing, while for model structures with thin capping layer the electron and hole are confined in the In-rich region, and the optical anisotropy is much less sensitive to the lateral alloy mixing.

I. INTRODUCTION

Optical properties of III-V semiconductor nanostructures have attracted a great deal of interest recently for their applications in optical communications that involve switching, amplification, and signal processings. $Ga_xIn_{1-x}As$ and $Ga_xIn_{1-x}P$ are among the most important ternary III-V compound semiconductors. The band gap of $Ga_xIn_{1-x}As$ covers both the 1.3 and 1.55 μm wavelengths, which are preferred in long distance fiber communications. However, long-wavelength photonic devices based on lattice-matched $Ga_{0.47}In_{0,53}As$/InP heterostructures suffer from strong Auger recombination and inter-valence band absorption processes[1-3]. Recently, to improve the performance of long-wavelength semiconductor lasers, long wavelength($\sim 1.55\mu$m) $Ga_xIn_{1-x}As$ quantum-wire (QWR) lasers have been grown by a single step molecular beam epitaxy technique[4-6].

An important optical property is the change in the emission of light (in energy, polarization, and intensity) that results from phase-space filling of carriers in one- and two-dimensionally (2D) confined systems. As the dimensionality of the quantum confinement increases from 1D to 2D, the sharpening of the density of states gives rise to a lower excitation threshold, thereby yielding potentially enhanced optical effects. It is found that the QWR laser structure is a promising candidate for optical communication device because of the many predicted benefits, such as higher gain, reduced temperature sensitivity, higher modulation bandwidths, and narrower spectral linewidths[5].

The fabrication of quantum wires via the strain-induced lateral-layer ordering (SILO) process starts with the growth of short-period superlattices (SPS) [e.g. $(GaAs)_2/(InAs)_{2.25}$] along the [001] direction. The excess fractional InAs layer leads to stripe-like islands during the MBE growth.[4] The presence of stripes combined with the strain effect lead to a natural phase separation as additional layers of GaAs or InAs are deposited. A self-assembled quantum wire heterostructure can then be created by sandwiching the composition modulated layer between barrier materials such as $Al_{0.24}Ga_{0.24}In_{0.52}As$ (quarternary), $Al_{0.48}In_{0.52}As$(ternary), or InP (binary)[4-6]. It was found that different barrier materials can lead to different degree of lateral composition modulation, and the consequent optical properties are different.[6] Besides the self-assembled lateral ordering, it is believed that the strain also plays a key role[5,6] in the temperature stability and optical anisotropy for the QWR laser structure. Much work has been undertaken which predicts that by using strained-layer superlattice to form the active region of a quantum-wire laser, the threshold current can be decreased by one order of magnitude, and the optical loss due to intervalence-band absorption and

Auger recombination will also be greatly reduced[4-6]. Also, the temperature sensitivity is reduced by an order of magnitude compared with strain-free structures. Temperature sensitivity of the lasing wavelength for typical GaInAs/InP lasers is around $5\mathring{A}/^0C$. By using a distributed-feedback structure, the temperature dependence of the lasing wavelength can be reduced to $1\mathring{A}/^0C$[5]. With the self-assembled GaInAs QWR, the temperature sensitivity is smaller than $0.1\mathring{A}/^0C$[5,6]. Thus, it represents an important improvement on the current technology in fabricating long wavelength lasers for fiber communication.

A few theoretical studies of $Ga_xIn_{1-x}As$ self-assembled QWRs based on a simplified uniform strain model have been reported.[8-10] In these calculations the SPS region is modeled by a $Ga_xIn_{1-x}As$ alloy with a lateral modulation of the composition x. Although these calculations can explain the QWR band gap and optical anisotropy qualitatively, it does not take into account the detailed SPS structure and the microscopic strain distribution. The understanding of these effects is important if one wish to have a full design capability of the self-assembled QWR optoelectronic devices. On the other hand, microscopic strain distributions in several SPS structures have been calculated, and the electronic properties of these SPS structures have been studied via an empirical pseudopotential method[11]. However, the effects of sandwiching the SPS structures between barrier materials so as to form QWRs have not been explored. It is also worth pointing out that the effective masses obtained in the pseudopotential method for the constituent bulk materials are $0.032m_0$ and $0.092m_0$ for InAs and GaAs, respectively.[12] These values are 30% larger than the actual values ($0.024m_0$ and $0.067m_0$); thus, the energy levels of quantum confined states obtained by this method are subject to similar uncertainty.

In this paper we present a systematic study of the effects of microscopic strain distribution on the electronic and optical properties of the $Ga_{1-x}In_xAs$ self-assembled QWRs via the combination of the effective bond-orbital model (EBOM) for electronic states and the valence-force-field (VFF) model for microscopic strain distribution. Both clamped and unclamped SPS structures with different degrees of lateral alloy mixing are considered. The clamped structure has a SPS layer sandwiched between the substrate and a thick capping layer so that the interface between the top monolayer of the SPS and the barrier region is atomically flat. The unclamped structures correspond to a SPS layer sandwiched between the substrate and a thin capping layer, which allows more flexible relaxation of interface atoms so the strain energy can be relieved. This leads to a wavy interface

structure. Most self-assembled QWR samples reported to date are closer to unclamped structures with a wavy interface, although it should be possible to produce self-assembled QWRs closer to the clamped structures by using a thick capping layer.

Our theoretical studies show that there are profound differences in the electronic and optical properties between the clamped and unclamped self-assembled QWR structures. In particular, we found that in clamped structures the electron and hole are confined in the Ga-rich region and the polarization of Photoluminescence (PL) can go from predominantly along [110] for SPS with abrupt change in In/Ga composition to predominantly along $[1\bar{1}0]$ for SPS with smooth change in In/Ga composition. On the other hand, for unclamped structures the electron and hole are confined in the In-rich region, and the optical polarization is always predominately along $[1\bar{1}0]$ with a weak dependence on the lateral alloy mixing. This also implies that by changing the degree of strain relaxation at the interface between the SPS and the capping layer, one can tailor the optical properties of self-assembled QWRs. Thus, through this theoretical study, we can gain a better understanding of the strain engineering of self-assembled QWR structures which may find applications in fiber-optical communication.

II. MODEL STRUCTURES

For both clamped and unclamped SPS structures, we consider different degrees of lateral alloy mixing and examine the effects of the microscopic strain distribution on the electronic and optical properties. Two example QWR model structures considered in the present paper (prior to alloy mixing) are depicted in Figure 1. The supercell of the first model structure consists of 8 pairs of (001) $(GaAs)_2/(InAs)_2$ SPS with a total thickness of $\approx 94\mathring{A}$ (quantum well region) followed by a $Al_{0.24}Ga_{0.24}In_{0.52}As$ layer (barrier region) with thickness $\approx 60\mathring{A}$ (20 diatomic layers). The supercell of the second model structure consists of 8 pairs of (001) $(GaAs)_2/(InAs)_{2.25}$ SPS with a total thickness of $\approx 100\mathring{A}$ (quantum well region) followed by a $Al_{0.24}Ga_{0.24}In_{0.52}As$ layer (barrier region). We assume an arrangement of alternating stripe like islands due to strain induced lateral ordering. In the diagram, no lateral alloy mixing is shown. In our calculations of strain distribution and electronic structures, different degrees of lateral alloy mixing will be considered. Experimentally, self-assembled InGaAs QWRs were usually grown with the (2/2.25) SPS structure.[12] However, the migration of excess In atoms during MBE growth could lead a structure somewhere between (2/2) SPS and

(2/2.25) SPS structures.

In both model structures, we can divide the self-assembled QWR into two regions with the left half being Ga rich and the right half In rich. During growth, varying degrees of lateral alloy mixing of these islands with the surround atoms is likely to occur. In the atomic layers with In-rich alloy filled the right half of the unit cell (layer 2 in structure 1 and layers 7 and 9 in structure 2), the In composition x_{In} is assumed to vary in the [110] direction (or y' direction) according to the relation

$$x_{In} = \begin{cases} x_m[1-\sin(\pi y'/2b)]/2 & \text{for } y' < b \\ 0 & \text{for } b < y' < L/2-b \\ x_m\{1+\sin[\pi(y'-L/2)/2b]\}/2 & \text{for } L/2-b < y' < L/2+b \\ x_m & \text{for } L/2+b < y' < L-b \\ x_m\{1-\sin[\pi(y'-L)/2b]\}/2 & \text{for } y' > L-b, \end{cases} \tag{1}$$

where x_m is the maximum In composition in the layer, $2b$ denotes the width of lateral composition grading, and L is the period of the lateral modulation in the [110] direction. In layer 4 of structure 1, which contains Ga-rich alloy in the left half of the unit cell, the Ga composition (x_{Ga}) as a function of y' is given by a similar equation with the sign of the sine function reversed as compared to Eq. (1). In structure 2, there are a few atomic layers that contain 0.25 monolayer of In (layers 3 and 13) or Ga(layers 5 and 11). The lateral alloy modulation in layers 3 and 13 is described by

$$x_{In} = \begin{cases} 0 & \text{for } 0 < y' < 5L/8-b \\ x_m\{1+\sin[\pi(y'-5L/8)/2b]\}/2 & \text{for } 5L/8-b < y' < 5L/8+b, \\ x_m & \text{for } 5L/8+b < y' < 7L/8-b \\ x_m\{1-\sin[\pi(y'-7L/8)/2b]\}/2 & \text{for } 7L/8-b < y' < 7L/8+b \\ 0 & \text{for } 7L/8+b < y' < L. \end{cases} \tag{2}$$

Similar equation for x_{Ga} in layers 5 and 11 can be deduced from the above. By varying the parameters x_m and b, we can get different degrees of lateral alloy mixing. Typically x_m is between 0.6 and 1, and b is between zero and $15a_{[110]} \approx 62\mathring{A}$.

A valence force field (VFF) model[13-15] is used to find the equilibrium atomic positions in the self-assembled QWR structure by minimizing the lattice energy. The strain tensor at each atomic (In or Ga) site is then obtained by calculating the local distortion of chemical bonds. We found that different local arrangement of atoms can lead to very different strain distribution. In particular,

the shear strain in the clamped structure can change substantially when the In/Ga composition modulation is changed. Consequently, the optical anisotropy can be reversed due to the change in the strength of the shear strain caused by the intermixing of In and Ga atoms.

III. THEORETICAL APPROACH

The method used in this paper for calculating the strained QWR band structure is based on the effective bond-orbital model (EBOM). A detailed description of this method has been published elsewhere[16,17]. EBOM is a tight binding-like model with minimum set of localized basis (the bonding or anti-bonding orbitals). The interaction and optical parameters are obtained by a correspondence with the $\mathbf{k}\cdot\mathbf{p}$ theory, which can be cast into analytic forms. Thus, the model can be viewed as a spatially discretized version of the $\mathbf{k}\cdot\mathbf{p}$ method, while retaining the virtues of LCAO (linear combination of atomic orbitals) method. The $\mathbf{k}\cdot\mathbf{p}$ model is the most popular one for treating electronic structures of semiconductor quantum wells or superlattices. However, when applied to complex structures such as self-assembled quantum wires[4-9] or quantum dots[13,18,19], the method becomes very cumbersome if one wish to implement the correct boundary conditions that take into account the differences in $\mathbf{k}\cdot\mathbf{p}$ band parameters for different materials involved. EBOM is free of this problem, since different material parameters are used at different atomic sites in a natural way. For simple structures, when both EBOM and $\mathbf{k}\cdot\mathbf{p}$ model are equally applicable, the results obtained are essentially identical.[16]

The optical matrix elements for the QWR states are computed in terms of elementary optical matrix elements between the valence-band bond orbitals and the conduction-band orbitals. The present calculation includes the coupling of the four spin-3/2 valence bands and the two spin-1/2 conduction bands closest to the band edges. Thus, it is equivalent to a 6-band $\mathbf{k}\cdot\mathbf{p}$ model. For our systems studied here, the band-edge properties are relatively unaffected by the split-off band due to the large spin-orbit splitting as discussed in our previous paper[9]. Hence, the split-off bands are ignored here. The bond-orbitals for the GaAs and InAs needed in the expansion of the superlattice states contain the following: four valence-band bond orbitals per bulk unit cell, which are p-like orbitals coupled with the spin to form orbitals with total angular momentum J=3/2 plus two conduction-band bond orbitals with J=1/2. They are written as

$$|\mathbf{R}, u_{JM}>=\sum_{\alpha,\sigma} C(\alpha,\sigma,J,M)|\vec{R},\alpha>\psi_\sigma, \tag{3}$$

where $J = 1/2$ and $3/2$ for the conduction and valence bands, respectively, and $M = -J, \cdots J$, ψ_σ, designates the electron spinor(σ=1/2,-1/2), and $|\mathbf{R}, \alpha>$ denote an α-like($\alpha = s, x, y, z$) bond orbital, located at unit cell $\mathbf{R}$. $C(\alpha, \sigma, J, M)$ are the coupling coefficients obtainable by group theory. All these bond orbitals are assumed to be sufficiently localized so that the interaction between orbitals separated farther than the nearest-neighbor distance can be ignored.

The effect of strain is included by adding a strain Hamiltonian H^{st} to the EBOM Hamiltonian[17]. The matrix elements of H^{st} in the bond-orbital basis can be obtained by the deformation-potential theory of Bir and Pikus[20]. We use the valence-force field (VFF) model of Keating[14] and Martin[15] to calculate the microscopic strain distribution. This model has been shown to be successful in fitting and predicting the elastic constants of elastic continuum theory, calculating strain distribution in a quantum well, and determining the atomic structure of III-V alloys. It was also used in the calculation of the strain distribution in self-assembled quantum dots.[13,19] The VFF model is a microscopic theory which includes bond stretching and bond bending, and avoids the potential failure of elastic continuum theory in the atomically thin limit. The total energy of the lattice is taken as

$$V = \frac{1}{4}\sum_{ij}\frac{3}{4}\alpha_{ij}(d_{ij}^2 - d_{0.ij}^2)^2/d_{0,ij}^2 + \frac{1}{4}\sum_i\sum_{j\neq k}\frac{3}{4}\beta_{ijk}(\vec{d_{ij}}.\vec{d_{ik}} + d_{0,ij}d_{0,ik}/3)^2/d_{0,ij}d_{0,ik} \tag{4}$$

where i runs over all the atomic sites, j, k run over the nearest-neighbor sites of i, $\vec{d_{ij}}$ is the vector joining the sites i and j, d_{ij} is the length of the bond, $d_{0,ij}$ is the corresponding equilibrium length in the binary constituents, and α_{ij} and β_{ijk} are the bond stretching and bond bending constants, respectively. α and β are from Martin's calculations.[11] For the bond-bending parameter β of In-As-Ga, we take $\beta_{ijk} = \sqrt{\beta[ij]\beta[ik]}$ following Ref. [15].

To find the strain tensor in the $InAs/GaAs$ self-assembled QWR, we start from ideal atomic positions and minimize the system energy using the Hamiltonian given above. Minimization of the total energy requires one to solve a set of coupled equations with 3N variables, where N is the total number of atoms. Direct solution of these equations is impractical in our case, since the system contains more than 6,000 atoms. We use an approach taken by several authors[10,13,19] which has been shown to be quite efficient. In the beginning of the simulation all the atoms are placed on the InP lattice, we allow atoms to deviate from this starting positions and use periodic boundary conditions in the plane perpendicular to the growth direction, while keeping atoms in the planes outside the

SPS region at their ideal atomic positions for a InP lattice (since the self-assembled QWR is grown epitaxially on the InP substrate). In each iteration, only one atomic position is displaced and other atom positions are held fixed. The direction of the displacement of atom i is determined according to the force $f_i = -\partial V/\partial x_i$ acting on it. All atoms are displaced in sequence. the whole sequence is repeated until the forces acting on all atoms become zero at which point the system energy is a minimum. Once the positions of all the atoms are known, the strain distribution is obtained through the strain tensor calculated according to the method described in Ref. [21].

Let R^0 be the position matrix without strain:

$$R^0 = \begin{pmatrix} R^0_{12x} & R^0_{23x} & R^0_{34x} \\ R^0_{12y} & R^0_{23y} & R^0_{34y} \\ R^0_{12z} & R^0_{23z} & R^0_{34z} \end{pmatrix},$$

where $\mathbf{R}^0_{ij} = \mathbf{R}^0_j - \mathbf{R}^0_i; i, j = 1, 4$ and $\mathbf{R}^0_i$ $(i = 1, 4)$ denote positions of four As atoms surrounding a Ga or In atom. Here we choose $\mathbf{R}^0_{12} = (1, -1, 0)a/2$, $\mathbf{R}^0_{23} = (-1, 0, -1)a/2$, and $\mathbf{R}^0_{34} = (1, 1, 0)a/2$. a is the lattice constant of GaAs or InAs, depending on the site. Let R be the corresponding position matrix with strain. It was shown in Ref. [21] that the strain tensor is given by

$$\epsilon = R * R_0^{-1} - 1. \tag{5}$$

After getting the strain tensor, the strain Hamiltonian is given by Bir and Pikus[20]

$$H^{st} = \begin{pmatrix} -\Delta V_H + D_1 & \sqrt{3}de_{xy} & \sqrt{3}de_{xz} \\ \sqrt{3}de_{xy} & -\Delta V_H + D_2 & \sqrt{3}de_{yz} \\ \sqrt{3}de_{xz} & \sqrt{3}de_{yz} & -\Delta V_H + D_3 \end{pmatrix}, \tag{6}$$

where $e_{ij} = (\epsilon_{ij} + \epsilon_{ji})/2$, and

$\Delta V_H = (a_1+a_2)(\epsilon_{xx}+\epsilon_{yy}+\epsilon_{zz})$, $D_1 = b(2\epsilon_{xx}-\epsilon_{yy}-\epsilon_{zz})$, $D_2 = b(2\epsilon_{yy}-\epsilon_{xx}-\epsilon_{zz})$, $D_3 = b(2\epsilon_{zz}-\epsilon_{yy}-\epsilon_{xx})$,

The strain potential on the s states is given by

$$\Delta V_c = c_1(\epsilon_{xx} + \epsilon_{yy} + \epsilon_{zz}),$$

The strain Hamiltonian in the bond-orbital basis $|JM>$ can be easily found by using the coupling constants[13], i.e,

$$< JM|H^{st}|J'M' >= \sum_{\alpha,\alpha',\sigma} C(\alpha,\sigma;J,M)^* C(\alpha',\sigma;J',M') H^{st}_{\alpha\alpha'} \quad (7)$$

The elastic constants C_{12} and C_{11} for GaAs, InAs and AlAs can be found in Ref. [22,23]. The deformation potentials $a_1,\ a_2,\ b,\ c_1,\ d$ can be found in Ref.[23-26]. The linear interpolation and virtual crystal approximations used to obtain the corresponding parameters for the barrier material ($Al_{0.24}Ga_{0.24}In_{0.52}As$).

The above strain Hamiltonian is derived locally for the each cation atom in the self-assembled QWR considered. To calculate the electronic states of the self-assembled QWR for model structure 1[see Fig. 1(a)], we first construct a zeroth-order Hamiltonian for a superlattice structure which contains in each period 8 pairs of (001) $(GaAs)_2/(InAs)_2$ SPS layers (with a total thickness around 100 Å) and 20 diatomic layers of $Al_{0.24}Ga_{0.24}In_{0.52}As$ (with thickness around 60 Å). So, the superlattice unit cell for the zeroth-order model contains 52 diatomic layers. The appropriate strain Hamiltonian for the the $(GaAs)_2/(InAs)_2$ SPS on InP is also included. For model structure 2 [see Fig. 1(b)], the zero-order superlattice consistes of two additional monolayers of InAs inserted into the 8 pairs of (2/2) SPS: one between the 2nd and 3rd pair of (2/2) SPS, the other between the 5th and 6th pair of (2/2) SPS.

The eigen-states for the zero-th order Hamiltonian for different values of k_2 (separated by the SL reciprocal lattice vectors in the [110] direction) are then used as the basis for calculating the self-assembled QWR electronic states. The difference in the Hamiltonian (including strain effects) caused by the intermixing of Ga and In atoms at the interfaces is then added to the zeroth-order Hamiltonian, and the electronic states of the full Hamiltonian is solved by diagonalizing the Hamiltonian matrix defined within a truncated set of eigen-states of the zeroth-order Hamiltonian. A total of ~ 500 eigen-states of the zero-th order Hamiltonian (with 21 different k_{110} points) were used in the expansion. The subbands closest to the band edge are converged to within 0.1 meV.

IV. RESULTS AND DISCUSSIONS

A. Strain distributions

In this section we discuss strain distributions in our model structures as described in section I with varying degree of lateral alloy mixing. Both clamped (with thick capping layer) and unclamped (with thin capping layer) situations are considered. To model the alloy structure with composition

modulation, we use a super-cell which contains 72 atoms in the [110] (y') direction, 36 atoms in the [1$\bar{1}$0] (x') direction and 64 or 68 atomic planes along the [001] (z) direction [8 pairs of (2/2) or (2/2.25) SPS] plus a GaAs capping layer. In the atomic planes which consist of alloy structure, we first determine the In composition at a given y' according to Eq. (1) and then use a random number generator to determine the atomic species along the x' direction. The bottom layer of atoms are bonded to the InP substrate with the substrate atoms fixed at their ideal atomic positions. The calculated strain distributions are then averaged over the x' coordinate. For the clamped case, the GaAs capping layer is assumed to be lattice matched to InP with a flat surface. For the unclamped case, the capping layer is allowed to relax freely, thus giving rise to a wavy surface structure.

The diagonal strains in the four atomic layers that constitute the (2/2) SPS in structure 1 for the clamped and unclamped cases are shown in Figs. 2 and 3, respectively. The lateral alloy modulation considered is described by Eq. (1) with $x_m = 0.8$ and $b = 7a_{[110]}$. For best illustration, we show diagonal strains in a rotated frame, in which x' is [1$\bar{1}$0], y' is [110], and z' is [001]. The layer number in the figure labels the atomic layers in Fig. 1(a), starting from the bottom layer as layer 1. There are two main features of the microscopic strain distribution. First, in the ideal situation (without atomic relaxation), one would predict $\epsilon_{y'y'}$ to be the same as $\epsilon_{x'x'}$ due to symmetry. However, with atomic relaxation, all Ga(In) atoms tend to shift in a direction so as to reduce the strain in the Ga(In)-rich region. Thus, the magnitude of $\epsilon_{y'y'}$ on Ga(In) sites (dashed lines) is lower(higher) than $\epsilon_{x'x'}$ in Ga(In)-rich region. Second, the z component strain (dash-dotted lines) tend to compensate the other two components such that the volume of each bulk unit cell is closer to that for the unstrained bulk. Thus, we see that $\epsilon_{z'z'}$ has an opposite sign compared to $\epsilon_{x'x'}$ or $\epsilon_{y'y'}$ at all atomic sites.

Comparing Fig. 2 with Fig. 3, we see that the main difference between the clamped and unclamped case is that in the atomic layers with lateral composition modulation (layers 2 and 4), the hydrostatic strain (sum of all three diagonal strain components) is much smaller in the unclamped structure than in the clamped structure. This would lead to a major difference in the band-edge profile for the two structures to be discussed below.

The difference in $\epsilon_{x'x'}$ and $\epsilon_{y'y'}$ leads to a nonzero shear strain $e_{xy} = (\epsilon_{y'y'} - \epsilon_{x'x'})/2$ in the original coordinates. For the clamped case, the shear strain is found to be particularly strong near the boundary where the alloy composition begins to change, and it is sensitive to the degree of lateral alloy mixing. For $x_m = 0.8$ and $b = 7a_{[110]}$, the maximum value of ϵ_{xy} is around 0.4% For abrupt

composition modulation ($x_m = 1$ and $b = 0$) the maximum ϵ_{xy} value increases five-fold to around 2%. The other shear strain components (ϵ_{xz} and ϵ_{yz}) are found to have similar magnitude. For the unclamped case, the shear strain is strong even in regions away from the boundary, and the maximum shear strain is larger than its counterpart in the clamped structure by about 30%.

The diagonal strains of structure 2 for the unclamped case with $x_m = 1$ and $b = 7a_{[110]}$ are shown in Fig. 4. The layer number in the figure labels the atomic layers in Fig. 1(b), starting from the bottom layer as layer 1. Only four representative atomic layers (3,4,5, and 7) are shown. We note that the average magnitude of the hydrostatic strain in the In-rich region in model structure 2 is comparable to that for unclamped structure 1.

B. Electronic structures

In order to understand the aspect of lateral quantum confinement due to composition modulation and strain, we examine the band-edge energies of a strained quantum well structure whose well material is the same structure as appeared in the SILO QWR with a fixed value of y' and the barrier is 60Åthick $Al_{0.24}Ga_{0.24}In_{0.52}As$ layer. For structure 1 depicted in Fig. 1(a), the well material consists of 8 pairs of $(GaAs)_2/(InAs)_2$ SPS. The conduction band minimum and valence band maximum of the above quantum well with different degrees of lateral alloy mixing as functions of y' (dashed lines) are shown in Fig. 5 for both clamped and unclamped cases. The strain Hamiltonian used here is the same as the one used in the self-assembled QWR at the corresponding y'. All material parameters are chosen the same as in Ref. [9] for temperature at 77K, except that the deformation potential c_1 of GaAs is slightly modified from $-6.8eV$ to $-7.1eV$ so that $a_1 + a_2 + c_1 = -9.8eV$ is in agreement with the experimental measurements[26] and the valence-band offset between GaAS and InAs used here is 0.26 eV according to the model solid theory[27]. To correct the band gap of SPS and alloy due to the bowing effect, we add a correction term $-0.4x(1-x)eV$ to the diagonal element for the s-like bond orbital in the Hamiltonian, where x is the effective alloy composition of the SPS or alloy at a given y'. With the correction of bowing effect, our model gives band gaps for the $(GaAs)_2(InAs)_2$ SPS, $Ga_{1-x}In_xAs$ alloy, and the superlattice made of $(GaAs)_2(InAs)_2$ SPS grown on InP substrate all in very good agreement with available experimental observations. The photoluminescence (PL) measurements indicates that the $(GaAs)_2(InAs)_2$ SPS grown on InP substrate has a gap around 0.75 eV.[28] Here we obtain a band gap of 0.74 eV for the $(GaAs)_2(InAs)_2$ SPS (with a strain distribution obtained again via the VFF model) and 0.79 eV for 8 pairs (or 100

Å) of $(GaAs)_2(InAs)_2$ SPS sandwiched between $Al_{0.24}Ga_{0.24}In_{0.52}As$ confining barriers. This is also consistent with the PL measurements on the $(GaAs)_2(InAs)_2$/InP multiple quantum wells.[28]

The band-edge profiles shown in this figure suggest that for the clamped case with alloy mixing, both electrons and holes are confined in the Ga-rich region with an effective barrier height around $0.13eV$ for the electron and $0.1eV$ for the hole. Both offsets are large enough to give rise to strong lateral confinement for electrons and holes in the Ga-rich region. Without alloy mixing, the electron is not well confined, since the average energy between the Ga-rich and In-rich regions are nearly the same. For the unclamped case, both electrons and holes are confined in the In-rich region with an effective barrier height around $0.2 - 0.3eV$ for the electron and $0.1 - 0.2eV$ for the hole. We note that the band gap in the In-rich region is rather insensitive to the alloy mixing, while the effective barrier height can change substantially due to different alloy mixing.

Fig. 6 shows the band-edge profiles for 8 pairs of (2/2.25) SPS [as illustrated in Fig. 1(b)] sandwiched between 60Å$Al_{0.24}Ga_{0.24}In_{0.52}As$ barriers with and without alloy mixing for both clamped and unclamped cases. For the clamped case, the electron is confined in the In-rich region, while the hole is confined in the Ga-rich region. Thus, we have a spatially indirect QWR, which will have very weak inter-band optical transition. For the unclamped case, the band-edge profile is similar to the unclamped case of structure 1 with both the electron and hole confined in the In-rich region. The band gaps for all cases of structure 2 are consistently smaller than their counterparts in structure 1.

Fig. 7 shows the near zone-center valence subband structures and squared optical matrix elements (P^2) for the QWR model structure 1 [as depicted in Fig. 1(a)] with thick capping layer (clamped case) and without alloy mixing. Here P^2 is defined as $\frac{2}{m_0}\sum_{s,s'} | < \psi_v|\hat{\epsilon}\cdot\mathbf{p}|\psi_c > |^2$, where ψ_v (ψ_c) denotes a valance (conduction) subband state. The symbol $\sum_{s,s'}$ means a sum over two near degenerate pair of subbands in the initial and final states. $\hat{\epsilon}$ denotes the polarization of light. Here we consider only the x' (along the QWR axis) and y' (perpendicular to the QWR axis) components. Only the dispersion along the k_1 ($[1\bar{1}0]$) direction is shown, since the dispersion along the k_2 direction for the confined levels is is rather small due to strong lateral confinement. All subbands are two-fold degenerate at the zone center due to the Kramer's degeneracy and they split at finite wave vectors as a result of lack of inversion symmetry in the system. The first three pairs of subbands are labeled V1, V2, and V3. They have unusually large energy separations compared with other valence subbands. This is because the first three pairs of subbands represent QWR confined states, whereas the other valence

subbands (with energies below -110 meV) are unconfined by the lateral composition modulation.

To examine the effects caused by the shear strain, we have also calculated the band structures with the shear strain set to zero. We found that without the shear strain the first pairs of valence subbands (V1) have much larger dispersion along the k_1 direction with an effective masses along $[1\bar{1}0]$ about a factor five smaller than that with the shear strain. This indicates that the V1 subband states for the case without shear strain are derived mainly from bond orbitals with x'-character, which leads to stronger overlap between two bond orbitals along the x' direction, hence larger dispersion along k_1. When the shear strain is present, the character of bond orbitals in the V1 subband states change from mainly x'-like to predominantly y'-like; thus, the dispersion along k_1 becomes much weaker. This explains the very flat V1 subbands as shown in Fig. 6. The switching of orbital character in the V1 subbands can be understood as follows. When the shear strain is absent, we have $\epsilon_{x'x'} = \epsilon_{y'y'}$, and the confinement effect in the y' direction pushes down the states with y' character (which has smaller effective mass in the y' direction), thus leaving the top valence subband (V1) to have predominantly x' character. On the other hand, with the presence of shear strain as shown in structure 1, we have $\epsilon_{y'y'} < \epsilon_{x'x'}$ in Ga-rich region, and the bi-axial term of the strain potential forces the y'-like states to move above the x'-like states, overcoming the confinement effect. As a result, the V1 subbands become y'-like. The conduction subbands are approximately parabolic as usual with a zone-center subband minimum equal to 688 meV This gives an energy gap of 763 meV for QWR model structure 1. As seen in this figure, the C1-V1 transition for y'-polarization (dashed line) is more than twice that for the x'-polarization (solid line) with $P^2_{[1\bar{1}0]}/P^2_{[110]} \approx 0.36$. This is consistent with the discussion for valence subband structures, where we concluded that the bond orbitals involved in the V1 subbands are predominantly y'-like.

Next, we study the case with alloy mixing, in which a gradual lateral modulation in In composition substantially reduces the shear strain. Using a lateral alloy mixing described in Eq. (1) with $x_m = 0.8$ and $b = 7a_{[110]}$, we found significant change in band structures and optical properties compared to the case without alloy mixing. With alloy mixing we found that the first pairs of valence subbands (V1) have much larger dispersion than their counterparts in Fig. 6, and the atomic character in the $V1$ states change from predominantly y'-like (without alloy mixing) to x'-like (with alloy mixing). The change of atomic character in the V1 states is a consequence of the competition between the QWR confinement (which suppresses the y' character) and the e_{xy} shear strain (which suppresses the

x' character). As a result, the ratio $P^2_{[1\bar{1}0]}/P^2_{[110]}$ changes from 0.36 (without alloy mixing) to 3.5 (with alloy mixing), indicating a reversal of optical anisotropy. The above studies lead to the conclusion that for self-assembled QWRs with thick capping layer (clamped case), the optical anisotropy is sensitive to the degree of lateral alloy mixing.

Next, we study the properties of self-assembled QWRs with thin capping layer (unclamped case). We found that for the unclamped case, the electron and hole are always confined in the In-rich region, regardless of the degree of alloy mixing and whether the QWR structure consists of (2/2) SPS or (2/2.25) SPS. Furthermore, since the strain in In-rich region has opposite sign compared to that in the Ga-rich region, the effect of shear strain on the VB states confined in In-rich region is also reversed. Namely, it pushes the energy of the y'-like VB states down relative to the x'-like VB states. Thus, both the QWR confinement and the shear strain effects are in favor of having a predominant x' character in the V1 subband. Therefore, the inter-band optical transition always has a ratio $P^2_{[1\bar{1}0]}/P^2_{[110]}$ larger than 1.

To illustrate this, we show in Fig. 8 the near zone-center valence subband structures and squared optical matrix elements (P^2) for the QWR model structure 1 [as depicted in Fig. 1(a)] with thin capping layer (unclamped case) and with alloy mixing described by $x_m = 0.8$ and $b = 7a_{[110]}$. Comparing the band structure in Fig. 8 with that in Fig. 7, we see that the V1 subband now has much larger dispersion (i.e. much smaller effective mass) than its counterpart in Fig. 6. There are two reasons for this. First, the hole in the unclamped case is now confined in the In-rich region rather than in the Ga-rich region as in the clamped case, thus having much smaller effective mass. Second, both the QWR confinement effect and the shear strain effect lead to a predominantly x' character in the V1 states, which tend to yield a smaller effective mass in the k_1 direction. The optical properties shown in Fig. 8 are also distinctly different from that shown in Fig. 7. The inter-band optical transition (C1-V1) now has a much stronger polarization along $[1\bar{1}0]$ than [110]. The quick drop of the the y' polarization in C1-V1 transition at $k_1 \approx 0.035\frac{2\pi}{a}$ is caused by the band mixing of V1 and V2 states as can be seen in the VB band structures in this figure.

We have also calculated the near zone-center valence subband structures and squared optical matrix elements (P^2) for the QWR model structure 2 with thin capping layer (not shown). We found that the band structures and optical matrix elements are similar to Fig. 8, except that the energy separation between V1 and V2 subbands are smaller (by $\sim 5mV$) and the polarization ratio

$(P^2_{[1\bar{1}0]}/P^2_{[110]})$ is larger.

Finally, we list in Table I the band gaps and the polarization ratio $(P^2_{[1\bar{1}0]}/P^2_{[110]})$ for various QWR structures with different degrees of lateral alloy mixing (as indicated by the parameters x_m and b). To calculate the polarization ratio in the photoluminescence (PL) spectra, we integrate the squared optical matrix element over the range of k_1 corresponding to the spread of exciton envelope function in the k_1 space. The exciton envelope function is obtained by solving the 1D Schrödinger equation for the exciton in the effective-mass approximation similar to what we did in Ref. 9. For unclamped (2/2) SPS structure, the band gap varies between 0.77 and 0.8 eV and the polarization ratio changes from 3.1 to 1.5 as the degree of alloy mixing is increased. For unclamped (2/2.25) SPS structure, both the band gap (around 0.74 eV) and the polarization ratio (around 2) are insensitive to the degree of alloy mixing.

Experimentally, the PL peak for self-assembled InGaAs QWRs with similar dimensions as considered in our model structures are around 735 meV and the polarization ratio for different samples are found to be between 2 and 4.[4-6] Taking into account an exciton binding energy between 10 and 20 meV, we find that our theoretical predictions for both unclamped and clamped structures with lateral alloy mixing are consistent with the experimental finding. To sort out which one is closer to the experimental structure would require more detailed comparison between the theory and experiment for optical spectra involving the excited hole states such as the PL excitation spectra.

V. CONCLUSION

We have calculated the band structures and optical matrix elements for the self-assembled GaInAs QWR grown by the SILO method. The actual SPS structure and the microscopic strain distribution has been taken into account. The effects of microscopic strain distribution on the valence subband structures and optical matrix elements are studied for two model self-assembled QWR structures, one with (2/2) SPS structure and the other with (2/2.25) SPS structure, and with varying degrees of lateral alloy mixing. The clamping effect due to thick capping layer is also examined. The valence force field (VFF) model is used to calculate the equilibrium atomic positions in the model QWR structures. This allows the calculation of the strain distribution at the atomistic level.

We found that in model structures with thick capping layer (clamped case), the magnitude of shear strain is quite large (around 2%) for abrupt lateral composition modulation and it reduces

substantially when the lateral alloy mixing is introduced. We found that the shear strain effect can alter the valence subband structures substantially when the hole is confined in the Ga-rich region, and it gives rise to a reversed optical anisotropy compared with QWR structures with negligible shear strain. This points to a possibility of "shear strain-engineering" to obtain QWR laser structures of desired optical anisotropy. For model structures with thin capping layer (unclamped case), the effect of shear strain is less dramatic, since the hole is confined in the In-rich region, where both the QWR confinement and the shear strain have similar effect. We found that polarization ratio ($P^2_{[1\bar{1}0]}/P^2_{[110]}$) for the unclamped case is always larger than 1 for both (2/2) and (2/2.25) SPS structures, regardless of the degree of lateral alloy mixing.

The band gap and polarization ratio obtained for both clamped and unclamped (2/2) SPS structures with lateral alloy mixing ($x_m \approx 0.8$) and for unclamped (2/2.25) SPS structures are consistent with experimental observations on most self-assembled InGaAs QWRs with similar specifications. For clamped (2/2) SPS structure without alloy mixing, we predicted a reversed optical anisotropy compared with the PL measurements for most InAs/GaAs self-assembled QWRs. However, there exist a few InAs/GaAs self-assembled QWR samples which display the reversed optical anisotropy at 77 K[7], and recent experimental studies also indicated a reversed optical anisotropy in many samples at 300 K.[6] Our studies demonstrated one possibility for the reversed optical anisotropy, the shear strain effect. There are other possibilities for the reversed optical anisotropy at 300K, such as the thermal population of the excited hole states, which can have different atomic characters as discussed in the previous section. The temperature dependence of the PL peak and polarization in self-assembled InGaAs QWRs[6] remains an intriguing question to be addressed in the future.

ACKNOWLEDGEMENTS

This work was supported in part by the National Science Foundation (NSF) under Grant No. NSF-ECS96-17153. S. Sun was also supported by a subcontract from the University of Southern California under the MURI program, AFOSR, Contract No. F49620-98-1-0474. We would like to thank K. Y. Cheng and D. E. Wohlert for fruitful discussions and for providing us with the detailed experimental data of the QWR structures considered here.

Table I. List of band gaps and polarization ratios for all structures studied

x_m	b/a_{110}	alloy mixing	clamped/unclamped	SPS structure	gap(eV)	$P_{\parallel}/P_{\perp}$
1.0	0	no	clamped	(2/2)	0.765	0.36
0.8	7	yes	clamped	(2/2)	0.763	3.5
1.0	0	no	unclamped	(2/2)	0.791	3.1
0.7	7	yes	unclamped	(2/2)	0.766	1.8
0.6	7	yes	unclamped	(2/2)	0.80	1.82
0.6	15	yes	unclamped	(2/2)	0.798	1.5
1.0	0	no	unclamped	(2/2.25)	0.731	2.2
1.0	7	yes	unclamped	(2/2.25)	0.74	2.1

REFERENCES

[1] A. R. Adams, Electron. Lett. **22**, 249 (1986).

[2] E. Yablonovitch and E. O. Kane. IEEE J. Lightwave Technol. LT-4, 504 (1986).

[3] G. P. Agrawa and N. K. Dutta, Long Wavelength Semiconductor Lasers, 2nd ed. (Van. Nostrand Reinhold, New York, 1993) Chap.7.

[4] S.T. Chou, K. Y. Cheng, L. J. Chou, and K. C. Hsieh, Appl. Phys. Lett. **17**, 2220 (1995); J. Appl. Phys. **78** 6270, (1995); J. Vac. Sci. Tech. B **13**, 650 (1995); K. Y. Cheng, K. C. Hsien, and J. N. Baillargeon, Appl. Phys. Lett. **60**, 2892 (1992).

[5] D. E. Wohlert, S. T. Chou, A. C Chen, K. Y. Cheng, and K. C. Hsieh, Appl. Phys. Lett. **17**, 2386 (1996).

[6] D.E. Wohlert, and K. Y. Cheng, Appl. Phys. Lett. **76**, 2249 (2000).

[7] D.E. Wohlert, and K. Y. Cheng, private communications.

[8] Y. Tang, H. T. Lin, D. H. Rich, P. Colter, and S. M. Vernon, Phys. Rev. B **53**, R10501 (1996).

[9] Y. Zhang and A. Mascarenhas, Phys. Rev. B**57**, 12245 (1998).

[10] L. X. Li and Y. C. Chang, J. Appl. Phys. **84** 6162, 1998.

[11] T. Mattila, L. Bellaiche, L. W. Wang, and A. Zunger, Appl. Phys. Lett., **72**, 2144 (1998).

[12] L. W. Wang, J. Kim, and A. Zunger, Phys. Rev. B **59**, 5678 (1999).

[13] H. Jiang and J. Singh, Phys. Rev. B**56**, 4696(1997).

[14] P. N. Keating, Phys. Rev. **145**, 637(1966).

[15] R. M. Martin, Phys. Rev. B**1**, 4005(1969).

[16] Y. C. Chang, Phys. Rev. B**37**, 8215 (1988).

[17] Mau-Phon Houng and Y.C Chang, J. Appl. Phys. **65**, 3096 (1989).

[18] M. Grundmann, O.Stier, and D. Bimberg, Phys. Rev. B **52**,11969 (1995).

[19] O.Stier, M.Grundmann, and D.Bimberg, Phys. Rev. B **59**, 5688,(1999).

[20] G. L. Bir and G. E. Pikus, Symmetry and Strain Induced Effects in Semiconductors (Halsted, United Kingdom, 1974); L.D. Landau and E. L. Lifshitz, Theory of Elasticity (Addison-Wesley Publishing Company Inc, Reading, Massachusetts, USA, 1970).

[21] C. Pryor, J. Kim, L.W. Wang, A.J. Williamson and A. Zunger, Phys. Rev. B**183**, 2548(1998).

[22] S. Adachi, J. Appl. Phys. **53**, 8775 (1982).

[23] H. Mathieu, P. Meroe, E. L. Amerziane, B. Archilla, J. Camassel, and G. Poiblaud, Phys. Rev. B**19**, 2209 (1979); S. Adachi and C. Hamaguchi, Phys. Rev. B**19**, 938 (1979).

[24] J. M. Hinckley and J. Singh, Phys. Rev. B**42**, 3546 (1990).

[25] O. Madelung and M. Schulz, Landolt-Börstein, New Series III/22a, p. 87 (1982).

[26] A. Blacha, H. Presting, M Cardona, Phys. Stat. Sol. (b) **126**, 11 (1984).

[27] C. G. Van de Walle, Phys. Rev. B **39**, 1871 (1989).

[28] M. Razeghi, Ph. Maurel, F. Omnes, and J. Nagle, Appl. Phys. Lett. **51**, 2216 (1987).

Figure Captions

Fig. 1. Schematic sketch of the unit cell of the SILO quantum wire for two model structures considered. Each unit cell consists of 8 pairs of (2/2) or (2/2.25) GaAs/InAs short-period superlattices (SPS). In structure 1, the (2/2) SPS contains four diatomic layers (only the cation planes are illustrated) and the SPS is repeated eight times. In structure 2, four pairs of (2/2.25) SPS (or 17 diatomic layers) form a period, and the period is repeated twice in the unit cell. Filled and open circles indicate Ga and In rows (each row extends infinitely along the $[1\bar{1}0]$ direction).

Fig. 2. Diagonal strain distribution of model structure 1 [corresponding to Fig. 1(a)] with thick capping layer (clamped case). Solid: $\epsilon_{x'x'}$. Dashed: $\epsilon_{y'y'}$. Dash-dotted: ϵ_{zz}. Parameters for alloy mixing: $x_m = 0.8$ and $b = 7a_{[110]}$.

Fig. 3. Diagonal strain distribution of model structure 1 with thin capping layer (unclamped case). Solid: $\epsilon_{x'x'}$. Dashed: $\epsilon_{y'y'}$. Dash-dotted: $\epsilon_{z'z'}$. Parameters for alloy mixing: $x_m = 0.8$ and $b = 7a_{[110]}$.

Fig. 4. Diagonal strain distribution of model structure 2 [corresponding to Fig. 1(b)] with thin capping layer (unclamped case). Solid: $\epsilon_{x'x'}$. Dashed: $\epsilon_{y'y'}$. Dash-dotted: $\epsilon_{z'z'}$. Parameters for alloy mixing: $x_m = 0.8$ and $b = 7a_{[110]}$.

Fig. 5. Conduction and valence band edges for 8 pairs of (2/2) SPS structures sandwiched between 60Å$Al_{0.24}Ga_{0.24}In_{0.52}As$ barriers with different degrees of lateral alloy mixing as functions of the [110] coordinate y' for both clamped (thick capping layer) and unclamped (thin capping layer) case. In upper pane, the dashed line is for abrupt modulation (without alloy mixing) and the solid line is for lateral alloy mixing with $x_m = 0.8$ and $b = 7a_{[110]}$. In lower panel, dash-dotted line: without alloy mixing; solid line: $x_m = 0.7$ and $b = 7a_{[110]}$; dotted lines: $x_m = 0.6$ and $b = 7a_{[110]}$; dashed lines: $x_m = 0.6$ and $b = 15a_{[110]}$.

Fig. 6. Conduction and valence band edges for 8 pairs of (2/2.25) SPS structures sandwiched between 60Å$Al_{0.24}Ga_{0.24}In_{0.52}As$ barriers with different degrees of lateral alloy mixing as functions of the [110] coordinate y' for both clamped (thick capping layer) and unclamped (thin capping layer) case. Dashed lines: without alloy mixing. Solid lines: with alloy mixing described by $x_m = 1.0$ and $b = 7a_{[110]}$.

Fig. 7. Valance subband structures and squared optical matrix elements for self-assembled QWR made of (2/2) SPS structure with thick capping layer (clamped case) and without alloy mixing.

Fig. 8. Valance subband structures and squared optical matrix elements for self-assembled QWR

made of (2/2) SPS structure with thin capping layer (unclamped case) and with alloy mixing described by $x_m = 0.8$ and $b = 7a_{[110]}$.

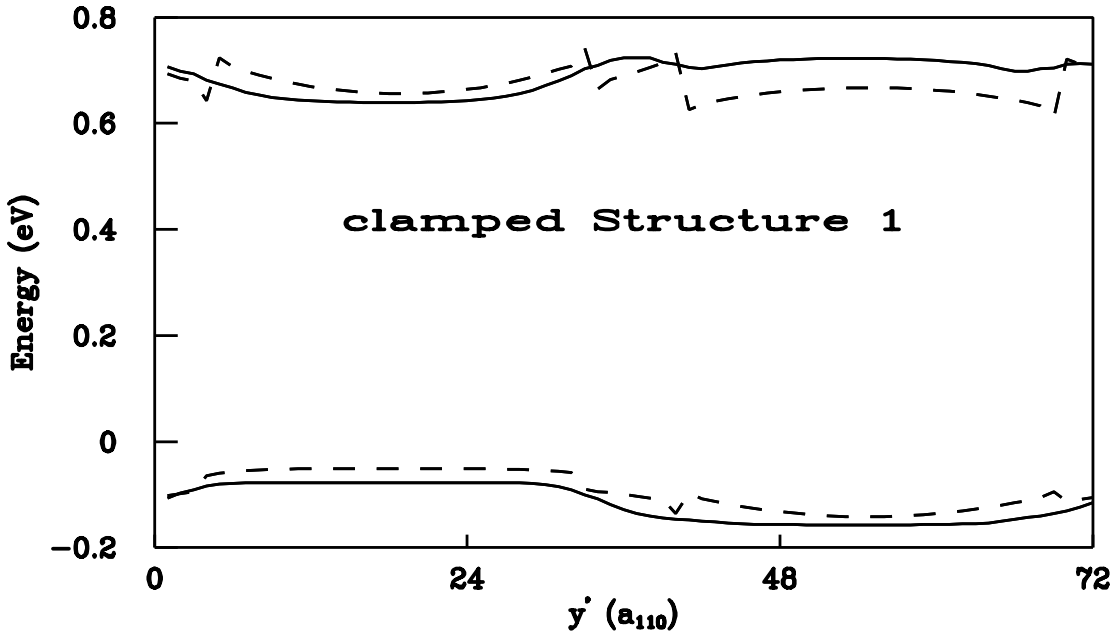
0.8
0.6
0.4
0.2
0
−0.2
Energy (eV)
clamped Structure 1
0
24
48
72
y' (a110)

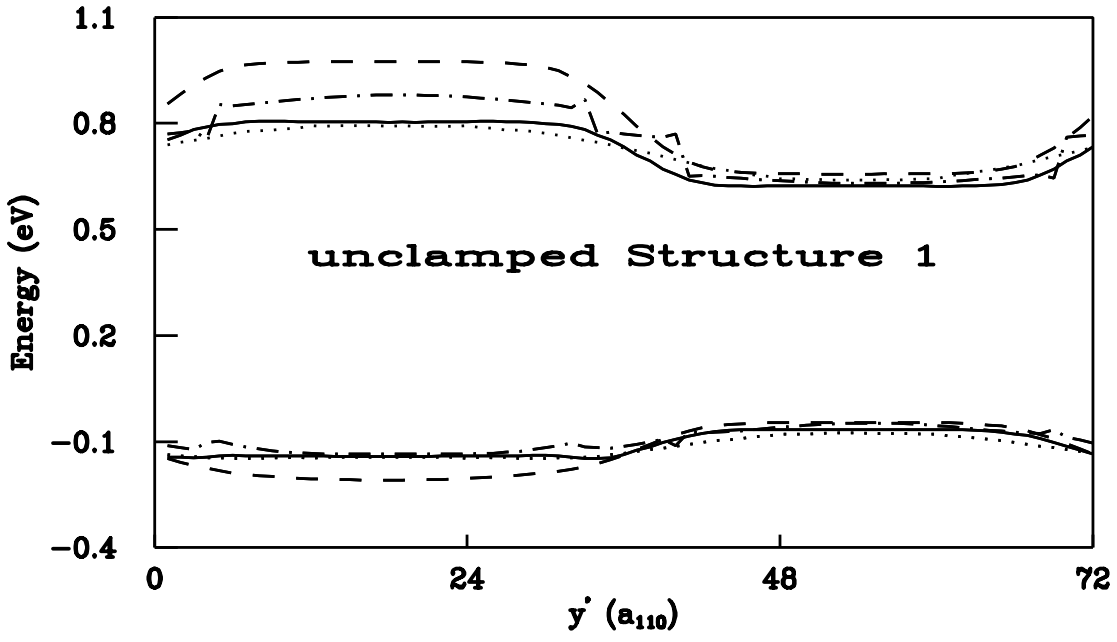
1.1
0.8
0.5
0.2
−0.1
−0.4
Energy (eV)
unclamped Structure 1
0
24
48
72
y' (a110)

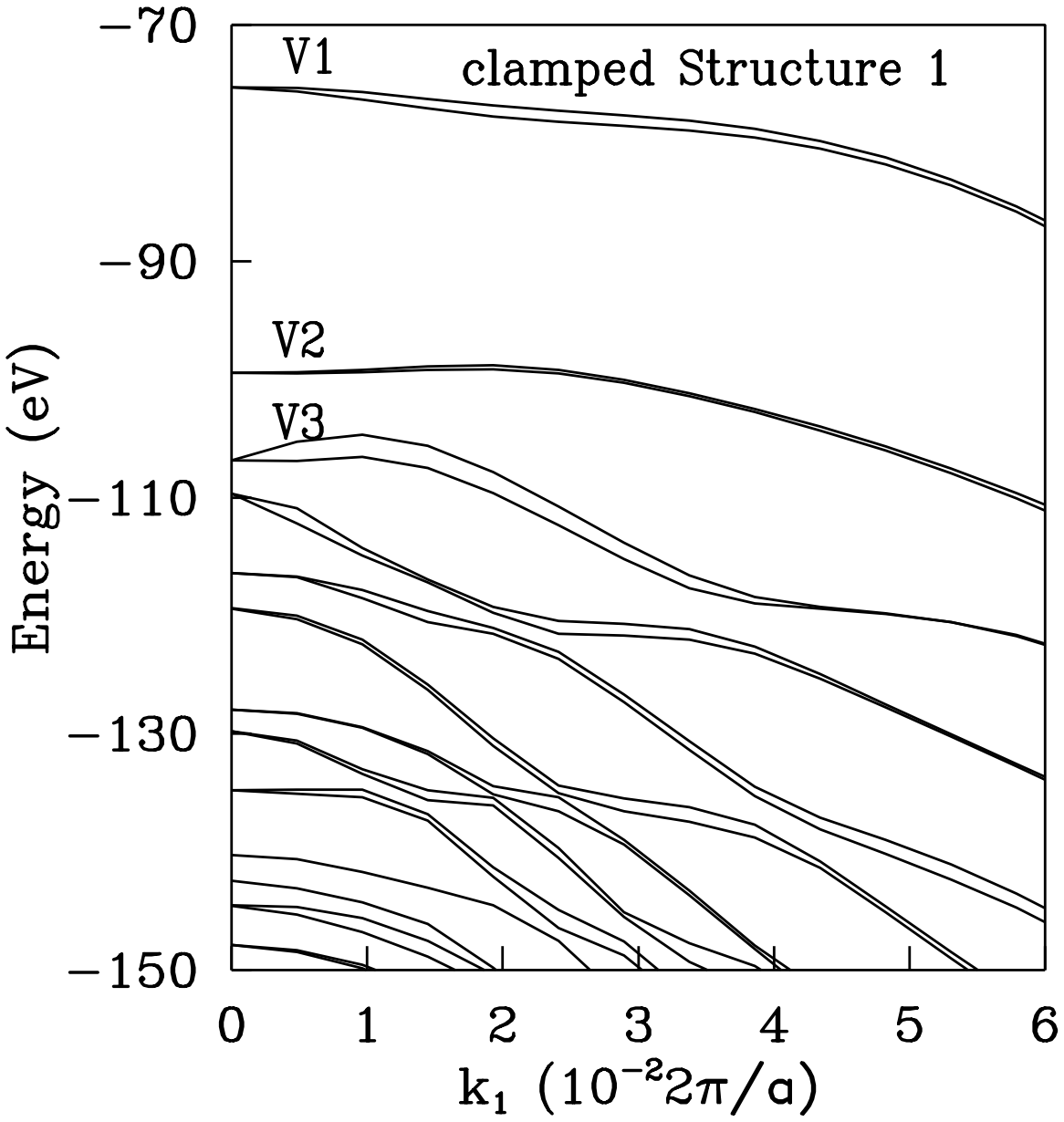
−70
−90
−110
−130
−150
Energy (eV)
V1
clamped Structure 1
V2
V3
0
1
2
3
4
5
6
k1 (10−2 2π/a)

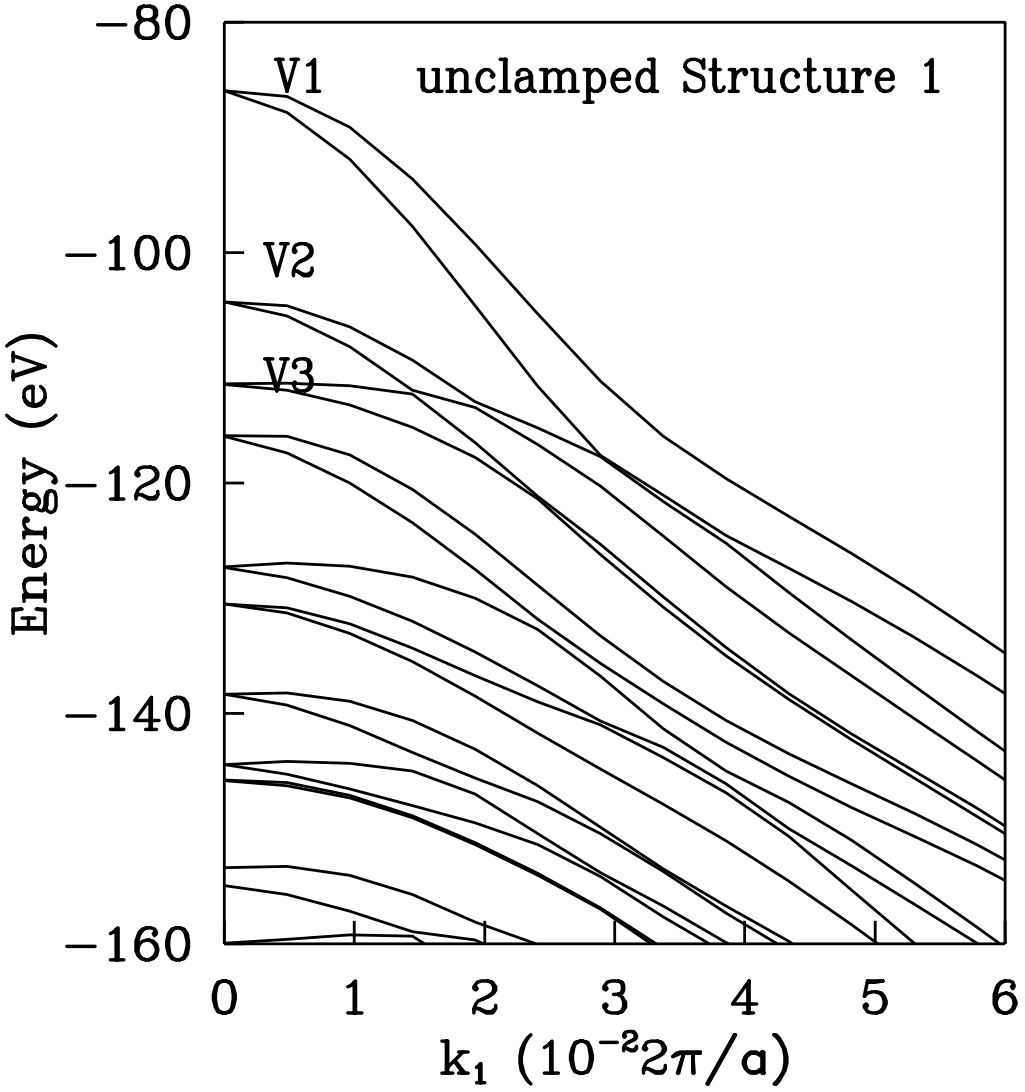
unclamped Structure 1
V1
V2
V3
−80
−100
−120
−140
−160
Energy (eV)
0
1
2
3
4
5
6
k1 (10−2 2π/a)

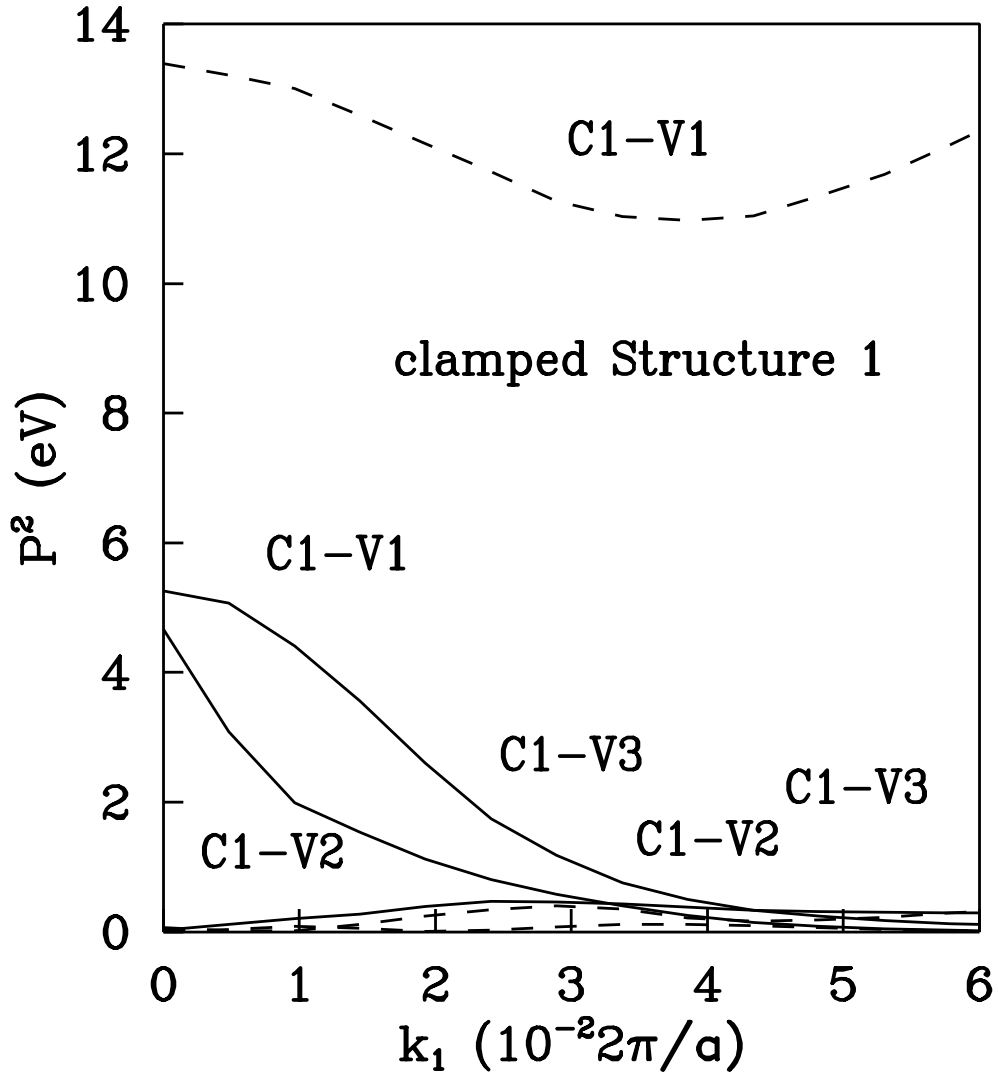
14
12
10
8
6
4
2
0
P² (eV)
C1−V1
clamped Structure 1
C1−V1
C1−V3
C1−V3
C1−V2
C1−V2
0
1
2
3
4
5
6
k₁ (10⁻²2π/a)

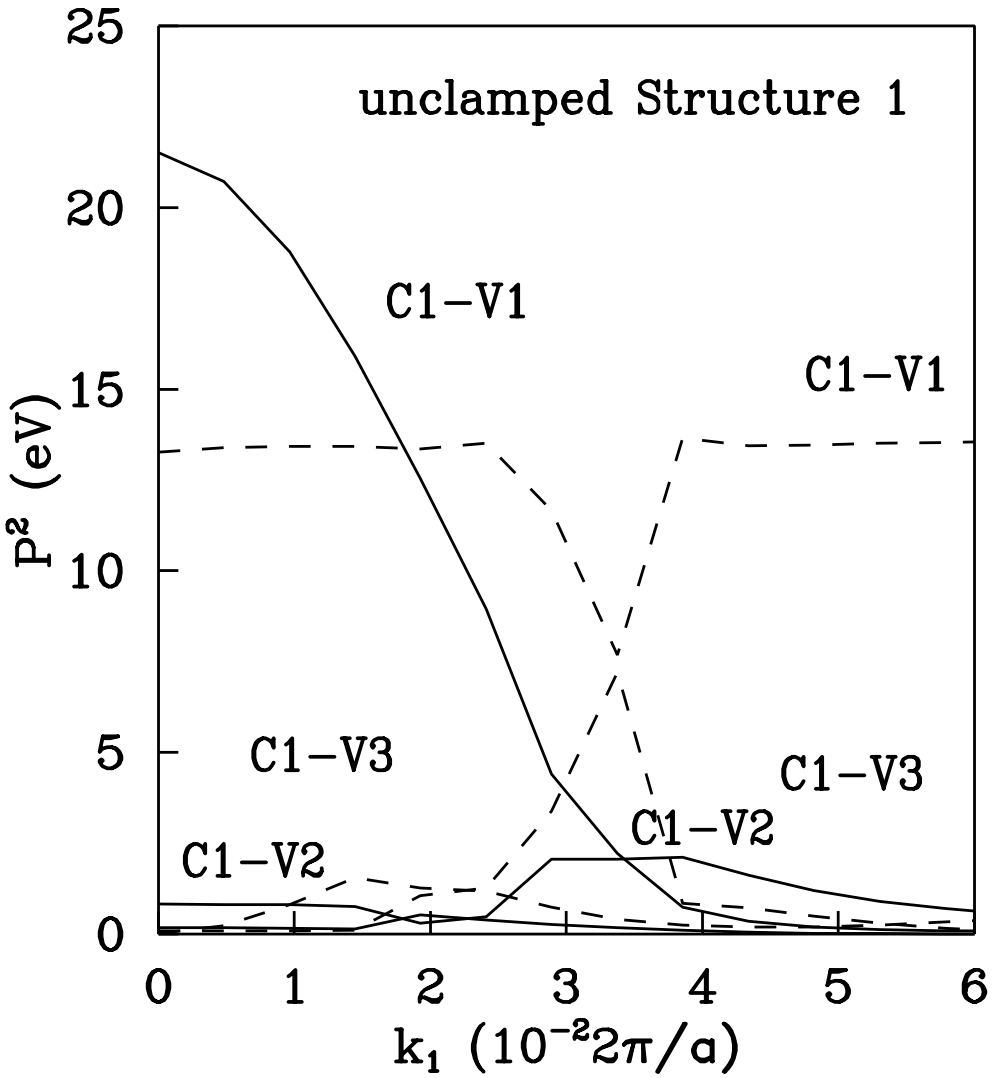
unclamped Structure 1
C1−V1
C1−V1
C1−V3
C1−V3
C1−V2
C1−V2
P² (eV)
k₁ (10⁻²2π/a)
0
5
10
15
20
25
0
1
2
3
4
5
6

Table.1 The list of results of all structures studied

x_m	b(a_{110})	alloy mixing	clamped/unclamped	structure model	gap(eV)	$P_{\|\|}/P_{\perp}$
1.0	0	no	clamped	1	0.765	0.36
0.8	7	yes	clamped	1	0.763	3.5
1.0	0	no	unclamped	1	0.791	3.1
0.7	7	yes	unclamped	1	0.766	1.8
0.6	7	yes	unclamped	1	0.80	1.82
0.6	15	yes	unclamped	1	0.798	1.5
1.0	0	no	unclamped	2	0.731	2.2
1.0	7	yes	unclamped	2	0.74	2.1

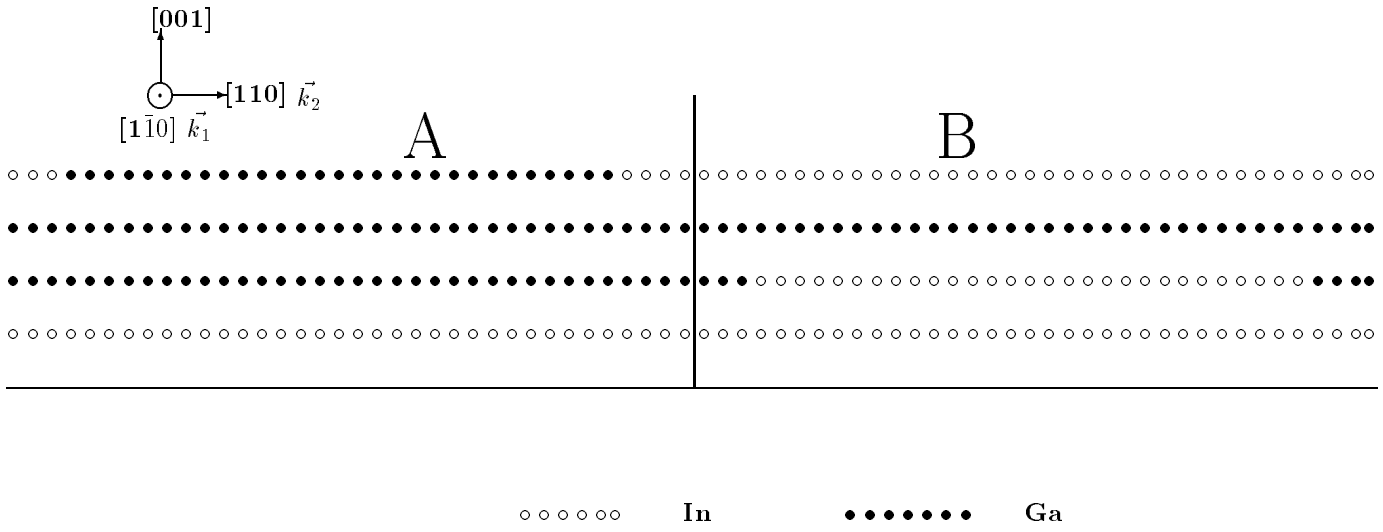

(a) Structure 1

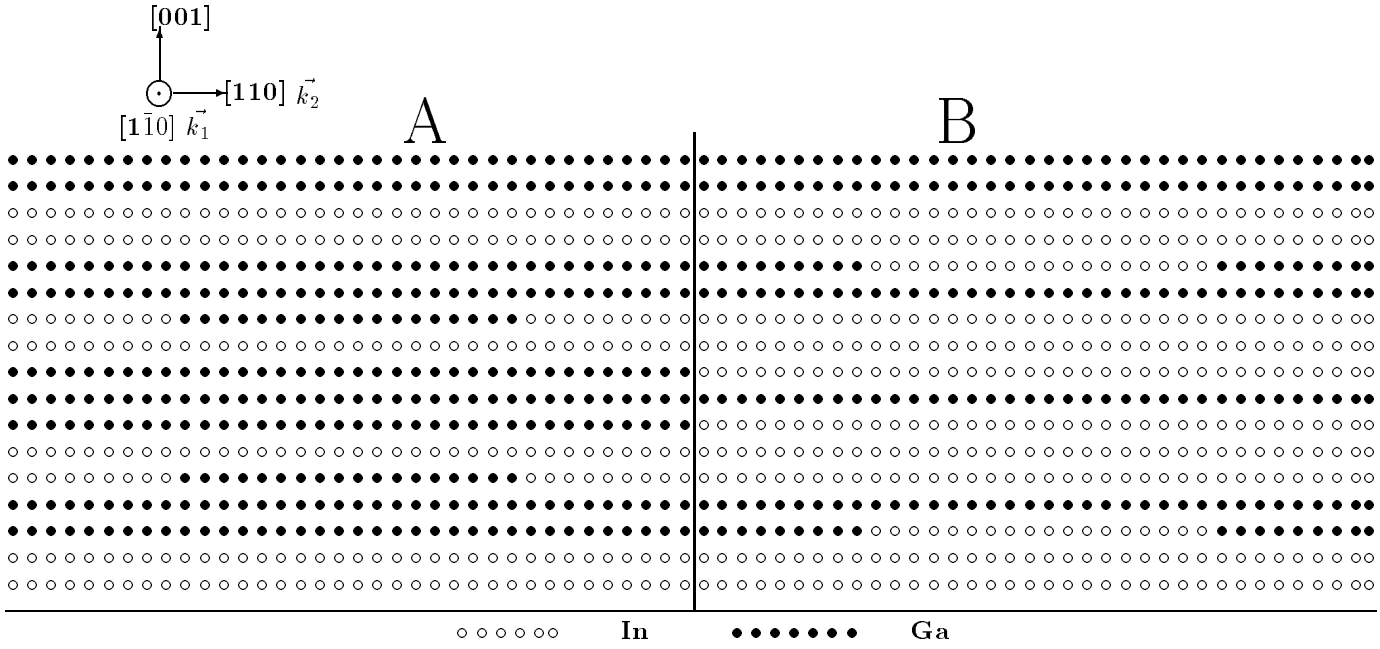

(b) Structure 2